THE ASTROPHYSICAL JOURNAL, 464:L1–L4, 1996 June 10

FOUR-YEAR *COBE*[1] DMR COSMIC MICROWAVE BACKGROUND OBSERVATIONS: MAPS AND BASIC RESULTS

C. L. BENNETT,[2] A. J. BANDAY,[3] K. M. GÓRSKI,[3] G. HINSHAW,[3] P. JACKSON,[3] P. KEEGSTRA,[3]
A. KOGUT,[3] G. F. SMOOT,[4] D. T. WILKINSON,[5] AND E. L. WRIGHT[6]
Received 1996 January 11; accepted 1996 March 21

ABSTRACT

In this Letter we present a summary of the spatial properties of the cosmic microwave background radiation based on the full 4 yr of *COBE* Differential Microwave Radiometer (DMR) observations, with additional details in a set of companion Letters. The anisotropy is consistent with a scale-invariant power-law model and Gaussian statistics. With full use of the multifrequency 4 yr DMR data, including our estimate of the effects of Galactic emission, we find a power-law spectral index of $n = 1.2 \pm 0.3$ and a quadrupole normalization $Q_{\rm rms-PS} = 15.3^{+3.8}_{-2.8}$ μK. For $n = 1$ the best-fit normalization is $Q_{{\rm rms-PS}|n=1} = 18 \pm 1.6$ μK. These values are consistent with both our previous 1 yr and 2 yr results. The results include use of the $\ell = 2$ quadrupole term; exclusion of this term gives consistent results, but with larger uncertainties. The final DMR 4 yr sky maps, presented in this Letter, portray an accurate overall visual impression of the anisotropy since the signal-to-noise ratio is ~2 per 10° sky map patch. The improved signal-to-noise ratio of the 4 yr maps also allows for improvements in Galactic modeling and limits on non-Gaussian statistics.

Subject headings: cosmic microwave background — cosmology: observations

1. INTRODUCTION

NASA's *COBE* Differential Microwave Radiometer (DMR) experiment (Smoot et al. 1990; Bennett et al. 1991) discovered cosmic microwave background (CMB) anisotropies based on its first year of data (Smoot et al. 1992; Bennett et al. 1992; Wright et al. 1992). The CMB temperature fluctuations were measured at an angular resolution of 7° at frequencies of 31.5, 53, and 90 GHz. These results were supported by a detailed examination of the DMR calibration and its uncertainties (Bennett et al. 1991) and a detailed treatment of the upper limits on residual systematic errors (Kogut et al. 1992). Bennett et al. (1992) showed that spatially correlated Galactic free-free and dust emission could not mimic the frequency spectrum nor the spatial distribution of the observed fluctuations. Bennett et al. (1993) also showed that the pattern of fluctuations does not spatially correlate with known extragalactic source distributions. Confirmation of the *COBE* results was attained by the positive cross-correlation between the *COBE* data and data from ground and balloon-borne observations (Ganga et al. 1993; Lineweaver et al. 1995). Bennett et al. (1994) reported the results from analyses of 2 yr of DMR data. The results from the 2 yr data were consistent with those from the first year alone. In this Letter we summarize the results and cosmological implications obtained from the full *COBE* DMR 4 yr data and provide references to further detailed reports of our analyses.

Primordial gravitational potential fluctuations were predicted to have an equal rms amplitude on all scales (Peebles & Yu 1970; Harrison 1970; Zeldovich 1972). This corresponds to a matter fluctuation power-law spectrum, $P(k) \propto k^n$, where k is the comoving wavenumber, with $n = 1$. Such a spectrum is also a natural consequence of inflationary models. If the effects of the transfer function of a standard cold dark matter model are included, *COBE* DMR should find $n_{\rm eff} \approx 1.1$ for a Peebles–Harrison-Zeldovich $n = 1$ universe. The power spectrum of the *COBE* DMR data is consistent with this.

A cosmological model does not predict the exact CMB temperature that would be observed in our sky, but rather predicts a statistical distribution of anisotropy parameters, such as spherical harmonic amplitudes. In the context of such models, the true CMB temperature observed in our sky is only a single realization from a statistical distribution. Thus, in addition to experimental uncertainties, we account for cosmic variance uncertainties in our analyses of the DMR maps. For a spherical harmonic temperature expansion $T(\theta, \phi) = \sum_{\ell m} a_{\ell m} Y_{\ell m}(\theta, \phi)$, cosmic variance is approximately expressed as $\sigma(C_\ell)/C_\ell \approx [2/(2\ell + 1)]^{1/2}$, where $C_\ell = \langle |a_{\ell m}|^2 \rangle$. Cosmic variance exists independent of the quality of the experiment. The power spectrum from the 4 yr DMR map is cosmic variance limited for $\ell \lesssim 20$.

This Letter includes a summary of the key results of a set of detailed DMR 4 yr analysis papers (Banday et al. 1996; Górski et al. 1996; Kogut et al. 1996a, 1996b, 1996c; Hinshaw et al. 1996a, 1996b; Wright et al. 1996).

2. OBSERVATIONS

DMR consists of six differential microwave radiometers: two nearly independent channels, labeled A and B, at frequencies 31.5, 53, and 90 GHz (wavelength 9.5, 5.7, and 3.3 mm). Each radiometer measures the difference in power between two 7° fields of view separated by 60°, 30° to either side of the spacecraft spin axis (Smoot et al. 1990). *COBE* was launched from Vandenberg Air Force Base on 1989 November 18 into a 900 km, 99° inclination circular orbit, which precesses to

[1] NASA/GSFC is responsible for the design, development, and operations of the *COBE*, and for the development of the analysis software and the delivery of the mission data sets. Scientific guidance is provided by the *COBE* Science Working Group.

[2] Laboratory for Astronomy and Solar Physics, Code 685, NASA/GSFC, Greenbelt, MD 20771; bennett@stars.gsfc.nasa.gov.

[3] Hughes STX Corporation, Laboratory for Astronomy and Solar Physics, Code 685, NASA/GSFC, Greenbelt, MD 20771.

[4] Department of Physics, Lawrence Berkeley Laboratory, Space Sciences Laboratory, and Center for Particle Astrophysics, Building 50-351, University of California, Berkeley, CA 94720.

[5] Physics Department, Jadwin Hall, Princeton University, Princeton, NJ 08544-1001.

[6] UCLA Astronomy, P.O. Box 951562, Los Angeles, CA 90095-1562.

follow the terminator. Attitude control keeps the spacecraft pointed away from Earth and nearly perpendicular to the Sun so that solar radiation never directly illuminates the aperture plane. The combined motions of the spacecraft spin (75 s period), orbit (103 m period), and orbital precession ($\sim$1° per day) allow each sky position to be compared to all others through a highly redundant set of temperature difference measurements spaced 60° apart. The on-board processor integrates the differential signal from each channel for 0.5 s, and records the digitized differences for daily playback to a ground station.

Ground data analysis consists of calibration, extensive systematic error analyses, and conversion of time-ordered data to sky maps (Kogut et al. 1996c). The DMR time-ordered data include systematic effects such as emission from Earth and the Moon, the instrument's response to thermal changes, and the instrument's response to Earth's magnetic field. The largest detected effects do not contribute significantly to the DMR maps: they are either on timescales that are long compared to the spacecraft spin sampling (e.g., thermal gain drifts) or have time dependence inconsistent with emission fixed on the celestial sphere (e.g., magnetic effects). Detected and potential systematic effects were quantitatively analyzed in detail by Kogut et al. (1996c). Data with the worst systematic contamination (lunar emission, terrestrial emission, and thermal gain changes) were not used in the map-making process and constitute less than 10% of the data in the 53 and 90 GHz channels. The remaining data were corrected using models of each effect. The data editing and correction parameters were conservatively chosen so that systematic artifacts, after correction, are less than 6 μK (95% confidence upper limit) in the final DMR map in the worst channel. This is significantly less than the levels of the noise and celestial signals.

We subtract a dipole [with Cartesian components (X, Y, Z) = (-0.2173, -2.2451, $+2.4853$) mK thermodynamic temperature in Galactic coordinates] from the time-ordered differential data prior to forming the 4 yr sky maps to reduce spatial gradients within a single pixel. A small residual dipole remains in the maps from a combination of CMB and Galactic emission. Figure 1 (Plate L1) shows the full sky maps at each frequency, after averaging the A and B channels, removing the CMB dipole, and smoothing to 10° effective resolution. The average 4 yr instrument noise, in mK antenna temperature per half-second observation for the 31A, 31B, 53A, 53B, 90A, and 90B channels are 58.27, 58.35, 69.66, 23.13, 27.12, 39.10, and 30.76, respectively.

The mean signal-to-noise ratios in the 10° smoothed maps are $\sim$0.5, 1.5, and 1.0 for 31, 53, and 90 GHz, respectively. For a multifrequency co-added map the signal-to-noise ratio is $\sim$2. This signal-to-noise level is adequate to portray an accurate overall visual impression of the anisotropy. This is illustrated in Figure 2 (Plate L2), where simulated data are shown in combination with the noise appropriate to 1, 2, and 4 yr of DMR 53 GHz observations.

Given the sensitivity of the 4 yr DMR maps we have chosen to extend the cut made in our previous analyses to exclude additional Galactic emission. Along with the previous $|b| < 20°$ exclusion zone, we use the *COBE* DIRBE 140 μm map as a guide to cut additional Galactic emission features. The full-sky DMR maps contain 6144 pixels. An optimum Galactic cut maximizes the number of remaining pixels while minimizing the Galactic contamination. Figure 3 shows the residual Galactic signal as a function of the number of usable pixels after a cut is applied based on the 140 μm DIRBE intensity. Our cut leaves 3881 pixels (in Galactic pixelization) while eliminating the strongest $|b| > 20°$ Galactic emission. Moderate changes to this custom cut will cause derived CMB parameters to change somewhat, but this is consistent with the data sampling differences of real CMB anisotropy features and not necessarily Galactic contamination. Solutions for $Q_{\rm rms-PS}$ typically increase by $\sim$1 μK with use of a $|b| < 20°$ cut compared the custom cut, while n is virtually unchanged. Likewise, derived CMB parameters also vary by the expected amount when the maps are made in ecliptic rather than Galactic coordinates since about one-half of the noise is rebinned.

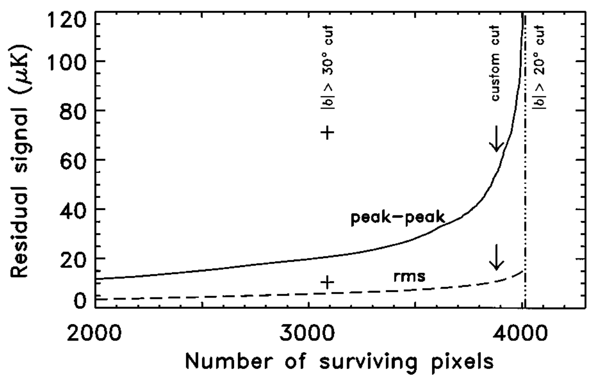

FIG. 3.—Estimated residual Galactic signal at 53 GHz as a function of the number of surviving map pixels after the application of an intensity cut that is based on the DIRBE 140 μm map. The conversion from DIRBE intensity to DMR 53 GHz intensity is from a correlation study (Kogut et al. 1996a). A minimum $|b| < 20°$ cut is always applied, leaving at most 4016 pixels. The arrows indicate the intensity cut that we chose to maximize the remaining number of pixels while minimizing the Galactic contamination. This leaves 3881 map pixels for CMB analysis. A simple $|b| < 30°$ cut produces the peak-to-peak intensity and rms shown by the plus (+) symbols, and is obviously less efficient than the custom cut.

Kogut et al. (1996a) examine the Galactic contamination of the surviving high Galactic latitude regions of the DMR maps after the "custom cut" (described above) is applied. No significant cross-correlation is found between the DMR maps and either the 408 MHz synchrotron map or the synchrotron map derived from a magnetic field model (Bennett et al. 1992). This places a 7° rms upper limit of $T_{\rm synch} < 11$ μK (95% confidence) on synchrotron emission at 31 GHz.

A significant correlation is found between the DMR maps and the dust-dominated DIRBE 140 μm map, with frequency dependence consistent with a superposition of dust and free-free emission. This corresponds to a 7° rms free-free emission component of 7.1 $\pm$ 1.7 μK at 53 GHz and a dust component of 2.7 $\pm$ 1.3 μK at 53 GHz. Since this emission is uncorrelated with CMB anisotropies it constitutes less than 10% of the CMB power. The amplitude of the correlated free-free component at 53 GHz agrees with a noiser estimate of free-free emission derived from a linear combination of DMR data that includes *all* emission with free-free spectral dependence. The combined dust and free-free emission contribute 10 $\pm$ 4 μK rms at both 53 and 90 GHz, $\approx$12% of the CMB power. These Galactic signal analyses are consistent with the fact that the fitted cosmological parameters are nearly unaffected by removal of modeled Galactic signals (Górski et al. 1996; Hinshaw et al. 1996a, 1996b), with the notable exception of the quadrupole, which has significant Galactic contamination (Kogut et al. 1996a). A search by Banday et al. (1996) finds no evidence for significant extragalactic contamination of the DMR maps.

3. INTERPRETATION

3.1. *Monopole $\ell = 0$*

Despite the fact that the DMR is a differential instrument, the known motion of the *COBE* spacecraft about Earth and the motion of Earth about the solar system barycenter allows a determination of the CMB monopole temperature from the DMR data. The CMB at millimeter wavelengths is well described by a blackbody spectrum (Mather et al. 1994; Fixsen et al. 1996). The Doppler effect from the combined spacecraft and Earth orbital motions creates a dipole signal $T(\theta) = T_0[1 + \beta \cos(\theta) + O(\beta^2)]$, where $\beta = v/c$ and θ is the angle relative to the time-dependent velocity vector. The satellite and Earth orbital motions are well known and change in a regular fashion, allowing their Doppler signal to be separated from fixed celestial signals. We fitted the time-ordered data to the Doppler dipole and recover a value for the CMB monopole temperature, $T_0 = 2.725 \pm 0.020$ K (Kogut et al. 1996c).

3.2. *Dipole $\ell = 1$*

The CMB anisotropy is dominated by a dipole term usually attributed to the motion of the solar system with respect to the CMB rest frame, as seen in Figure 4 (Plate L3). A precise determination of the dipole must account for Galactic emission and the aliasing of power from higher multipole orders once pixels near the Galactic plane are discarded. We account for Galactic emission using a linear combination of the DMR maps or by cross-correlating the DMR maps with template sky maps dominated by Galactic emission (Kogut et al. 1996a). We fitted the high-latitude portion of the sky for a dipole with a CMB frequency spectrum using a pixel-based likelihood analysis (Hinshaw et al. 1996b). Accounting for the smoothing by the DMR beam and map pixelization, the CMB dipole has amplitude of 3.353 ± 0.024 mK toward Galactic coordinates $(l, b) = (264°.26 \pm 0°.33, 48°.22 \pm 0°.13)$ or equatorial coordinates $(\alpha, \delta) = (11^h12^m.2 \pm 0^m.8, -7°.06 \pm 0°.16)$ epoch J2000.

3.3. *Quadrupole $\ell = 2$*

For the quadrupole, Galactic emission is comparable in amplitude to the anisotropy in the CMB. We use a likelihood analysis to fit the high-latitude portion of the DMR maps for Galactic emission traced by synchrotron- and dust-dominated surveys and a quadrupole anisotropy with a thermodynamic frequency spectrum (Kogut et al. 1996a; Hinshaw et al. 1996b). The quadrupole amplitude is $Q_{\rm rms} = 10.0^{+7}_{-4}$ μK (68% confidence). The observed quadrupole amplitude, $Q_{\rm rms}$, has a lower value than the quadrupole expected from a power-law fit to the entire power spectrum, $Q_{\rm rms-PS} = 15.3^{+3.8}_{-2.8}$ μK (discussed below). This difference is consistent with cosmic variance.

3.4. *Power Spectrum $\ell \geq 2$*

The simplest probe of the angular power spectrum of the anisotropy is its Legendre transform, the two-point correlation function. The two-point correlation function of the 4 yr maps is analyzed by Hinshaw et al. (1996a), where it is shown that the two-point data are consistent from channel to channel and frequency to frequency. The data are robust with respect to the angular power spectrum. As in Bennett et al. (1994), we use a Monte Carlo–based Gaussian likelihood analysis to infer the most likely quadrupole normalization for a scale-invariant ($n = 1$) power-law spectrum. The results are summarized in Table 1, where we also include the results of three additional, independent power spectrum analyses, discussed below. The normalization inferred from the two-point function is now in better agreement with other determinations than was the case with the 2 yr data. The change is due to data selection: with the 2 yr data, we analyzed only the 53×90 GHz cross-correlation function; with the 4 yr data we have analyzed many more data combinations, including the autocorrelation of a co-added, multifrequency map. This latter combination is more comparable to the data analyzed by other methods, and the two-point analysis yields consistent results in that case.

TABLE 1

DMR 4 YEAR POWER SPECTRUM SUMMARY

Statistic	Reference	n [a]	$Q_{\rm rms-PS}$ [a] (μK)	$Q_{\rm rms-PS \mid n=1}$ [b] (μK)
No Galaxy Correction[c]				
Two-point function	1	...	...	$18.6^{+1.4}_{-1.4}$
Orthogonal functions	2	$1.23^{+0.23}_{-0.29}$	$15.3^{+3.9}_{-2.6}$	$18.3^{+1.3}_{-1.2}$
Pixel temperature	3	$1.25^{+0.26}_{-0.29}$	$15.4^{+3.9}_{-2.9}$	$18.4^{+1.4}_{-1.3}$
Hauser-Peebles	4	$1.30^{+0.30}_{-0.34}$	...	$17.7^{+1.4}_{-1.8}$
DIRBE-Template Galaxy Correction[d]				
Two-point function	1	...	...	$17.5^{+1.4}_{-1.4}$
Orthogonal functions	2	$1.21^{+0.24}_{-0.28}$	$15.2^{+3.7}_{-2.6}$	$17.7^{+1.3}_{-1.2}$
Pixel temperatures	3	$1.23^{+0.26}_{-0.27}$	$15.2^{+3.6}_{-2.8}$	$17.8^{+1.3}_{-1.3}$
Hauser-Peebles	4	...	...	...
Internal Combination Galaxy Correction[e]				
Two-point function	1	...	...	$16.7^{+2.0}_{-2.0}$
Orthogonal functions	2	$1.11^{+0.38}_{-0.42}$	$16.3^{+5.2}_{-3.7}$	$17.4^{+1.8}_{-1.7}$
Pixel temperatures	3	$1.00^{+0.40}_{-0.43}$	$17.2^{+5.6}_{-4.0}$	$17.2^{+1.9}_{-1.7}$
Hauser-Peebles	4	$1.62^{+0.44}_{-0.50}$	...	$19.6^{+2.5}_{-2.5}$

REFERENCES.—(1) Hinshaw et al. 1996a; (2) Górski et al. 1996; (3) Hinshaw et al. 1996b; (4) Wright et al. 1996; data selection differs slightly in the case of Wright et al., as described in the reference

[a] Mode and 68% confidence range of the projection of the two-dimensional likelihood, $L(Q, n)$, on n or Q.

[b] Mode and 68% confidence range of the slice of the two-dimensional likelihood, $L(Q, n)$, at $n = 1$.

[c] Formed from the weighted average of all six channels.

[d] Formed from the weighted average of all six channels with the best-fit Galactic template maps subtracted (Kogut et al. 1996a).

[e] Formed from a linear combination of all six channel maps that cancels free-free emission (Kogut et al. 1996).

It is also possible to analyze the power spectrum directly in terms of spherical harmonics. However, there is considerable subtlety in this because the removal of the Galactic plane renders the harmonics nonorthonormal, producing strong correlations among the fitted amplitudes. Wright et al. (1996) has solved for an angular power spectrum by modifying and applying the technique described by Peebles (1973) and Hauser & Peebles (1973) for data on the cut sphere. They compute a Gaussian likelihood on these data and calibrate their results with Monte Carlo simulations. Górski et al. (1996) explicitly construct orthonormal functions on the cut sphere and decompose the anisotropy data with respect to these modes. They form and evaluate an exact Gaussian likelihood directly in terms of this mode decomposition. The results of these analyses are summarized in Table 1. Further details, including results from other data combinations are given in the respective papers.

Hinshaw et al. (1996b) evaluate a Gaussian likelihood directly in terms of a full pixel-pixel covariance matrix, a technique applied to the 2 yr data by Tegmark & Bunn (1995). The results of the power-law spectrum fits are summarized in Table 1. Hinshaw et al. (1996b) also analyze the quadrupole anisotropy separately from the higher order modes to complement the analysis of Kogut et al. (1996a). They compute a likelihood for the quadrupole mode C_2, nearly independent of higher order power and show that it peaks between 6 and 10 μK, depending on Galactic model, but that its distribution is so wide that it is easily consistent with $15.3^{+3.8}_{-2.8}$ μK, the value derived using the full power spectrum.

3.5. *Tests for Gaussian Statistics*

It is important to determine whether the primordial fluctuations are Gaussian. The probability distribution of temperature residuals should be close to Gaussian if the sky variance is Gaussian and the receiver noise is Gaussian. The receiver noise varies somewhat from pixel to pixel because the observation times are not all the same, but when this is taken into account the data appear Gaussian (Smoot et al. 1994). There is no evidence for an excess of large deviations, as would be expected if there were an unknown population of point sources. A search for point sources in the 2 yr maps was negative (Kogut et al. 1994). Given the large beam of the instrument and the variance of both cosmic signals and receiver noise, it is still possible for interesting signals to be hidden in the data.

Kogut et al. (1996b) compare the 4 yr DMR maps to Monte Carlo simulations of Gaussian power-law CMB anisotropy. The three-point correlation function, the two-point correlation of temperature extrema, and the topological genus are all in excellent agreement with the hypothesis that the CMB anisotropy on angular scales of 7° or larger represents a random-phase Gaussian field. Kogut et al. (1996b) examine the alternate hypothesis that the CMB is a random realization of a field whose spherical harmonic coefficients are drawn from a χ^2 distribution with N degrees of freedom. Testing this against the DMR maps, they find that not only do Gaussian power-law models provide an adequate description of the large-scale CMB anisotropy, but non-Gaussian models with $1 < N < 60$ are 5 times less likely to describe the true statistical distribution than the exact Gaussian model. While this does not test the infinite range of possible non-Gaussian models, the DMR data can be used to constrain specific models.

4. SUMMARY OF FOUR-YEAR *COBE* DMR CMB MEASUREMENTS

1. The full 4 yr set of *COBE* DMR observations is analyzed and full-sky maps are presented. The typical signal-to-noise ratio in a 10° smoothed map is ~2 in the frequency-averaged map, enough to provide a visual impression of the anisotropy.

2. We derive a CMB monopole temperature from DMR (despite its being a differential instrument) of $T_0 = 2.725 \pm 0.020$ K (Kogut et al. 1996c). This is in excellent agreement with the *COBE* FIRAS precision measurement of the spectrum of the CMB, $T_0 = 2.728 \pm 0.002$ K (Fixsen et al. 1996).

3. The CMB dipole from DMR has amplitude 3.353 ± 0.024 mK toward Galactic coordinates $(l, b) = (264\overset{\circ}{.}26 \pm 0\overset{\circ}{.}33,\ 48\overset{\circ}{.}22 \pm 0\overset{\circ}{.}13)$, or equatorial coordinates $(\alpha, \delta) = (11^{h}12\overset{m}{.}2 \pm 0\overset{m}{.}8,\ -7\overset{\circ}{.}06 \pm 0\overset{\circ}{.}16)$ epoch J2000. This is consistent with the dipole amplitude and direction derived by *COBE* FIRAS (Fixsen et al. 1996).

4. The quadrupole amplitude is $Q_{\rm rms} = 10.0^{+7}_{-4}$ μK (68% confidence) and the 95% confidence interval quadrupole amplitude is 4 $\mu K \le Q_{\rm rms} \le 28$ μK. This is consistent with the value predicted by a power-law fit to the power spectrum: $Q_{\rm rms-PS} = 15.3^{+3.8}_{-2.8}$ μK (Kogut et al. 1996a; Hinshaw et al. 1996b).

5. The power spectrum of large angular scale CMB measurements are consistent with an $n = 1$ power law (Górski et al. 1996; Hinshaw et al. 1996b; Wright et al. 1996). If the effects of a standard cold dark matter model are included, *COBE* DMR should find $n_{\rm eff} \approx 1.1$ for an $n = 1$ universe.) With full use of the multifrequency 4 yr DMR data, including our estimate of the effects of Galactic emission, we find a power-law spectral index of $n = 1.2 \pm 0.3$ and a quadrupole normalization $Q_{\rm rms-PS} = 15.3^{+3.8}_{-2.8}$ μK. For $n = 1$ the best-fit normalization is $Q_{\rm rms-PS}|_{n=1} = 18 \pm 1.6$ μK. Differences in the derived values of Q and n between various analyses of DMR data are much more dependent on the detailed data selection effects than on the analysis technique. The combined 31, 53, and 90 GHz 10° smoothed CMB rms is 29 ± 1 μK.

6. The DMR anisotropy data are consistent with Gaussian statistics. Statistical tests prefer Gaussian over other toy statistical models by a factor of ~5 (Kogut et al. 1996b).

The DMR time-ordered data, map data, and ancillary data sets (including our custom Galactic cut) are publicly available through the National Space Science Data Center (NSSDC) at http://www.gsfc.nasa.gov/astro/cobe/cobe_home.html. We gratefully acknowledge the *COBE* support provided by the NASA Office of Space Sciences (OSS). We also acknowledge the contributions of J. Aymon, V. Kumar, R. Kummerer, C. Lineweaver, J. Santana, and L. Tenorio.

REFERENCES

Banday, A., et al. 1996, ApJ, submitted
Bennett, C. L., et al. 1991, ApJ, 391, 466
———. 1992, ApJ, 396, L7
———. 1993, ApJ, 414, L77
———. 1994, ApJ, 436, 423
Fixsen, D. J., et al. 1996, ApJ, submitted
Ganga, K., et al. 1993, ApJ, 410, L57
Górski, K. M., et al. 1996, ApJL, 464, L11
Harrison, E. R. 1970, Phys. Rev. D, 1, 2726
Hauser, M. G., & Peebles, P. J. E. 1973, ApJ, 185, 757
Hinshaw, G., Banday, A. J., Bennett, C. L., Górski, K. M., Kogut, A., Lineweaver, C. H., Smoot, G. F., & Wright, E. L. 1996a, ApJL, 464, L25
Hinshaw, G., Banday, A. J., Bennett, C. L., Górski, K. M., Kogut, A., Smoot, G. F., & Wright, E. L. 1996b, ApJL, 464, L17
Kogut, A., Banday, A. J., Bennett, C. L., Górski, K. M., Hinshaw, G., Smoot, G. F., & Wright, E. L. 1996a, 464, L5
———. 1996b, 464, L29
Kogut, A., Banday, A. J., Bennett, C. L., Hinshaw, G., Loewenstein, K., Lubin, P., Smoot, G. F., & Wright, E. L. 1994, ApJ, 433, 435
Kogut, A., et al. 1992, ApJ, 401, 1
———. 1996c, ApJ, in press
Lineweaver, C. H., et al. 1995, ApJ, 448, 482
Mather, J. C., et al. 1994, ApJ, 420, 439
Peebles, P. J. E. 1973, ApJ, 185, 413
Peebles, P. J. E., & Yu, J. T. 1970, ApJ, 162, 815
Smoot, G. F., et al. 1990, ApJ, 360, 685
———. 1992, ApJ, 396, L1
Smoot, G. F., Tenorio, L., Banday, A. J., Kogut, A., Wright, E. L., Hinshaw, G., & Bennett, C. L. 1994, ApJ, 437, 1
Tegmark, M., & Bunn, E. F. 1995, ApJ, 455, 1
Wright, E. L., et al. 1992, ApJ, 396, L13
———. 1996, ApJL, 464, L21
Zeldovich, Ya B. 1972, MNRAS, 160, 1

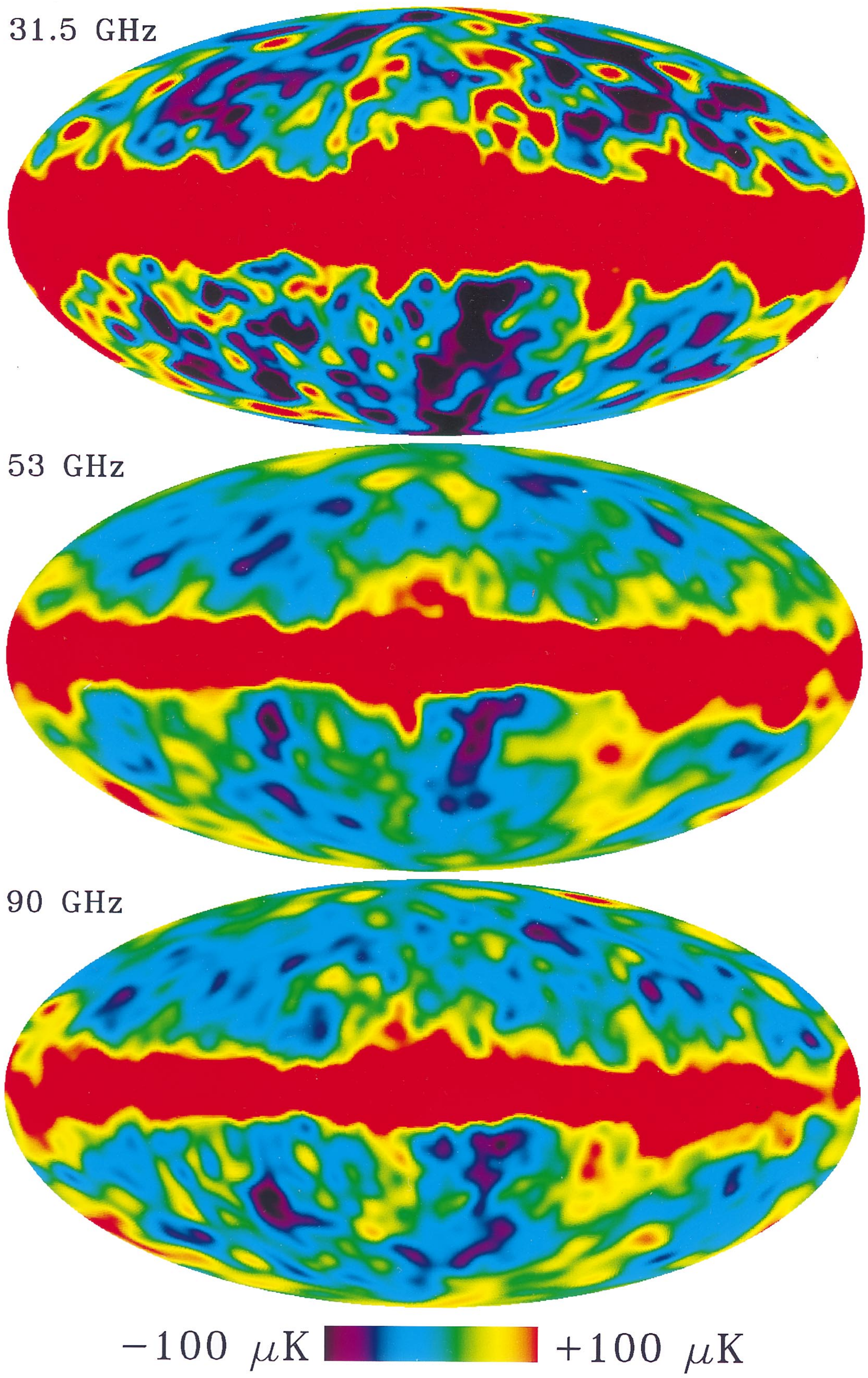

FIG. 1.—Full-sky Mollweide projections of the 31, 53, and 90 GHz 4 yr maps formed by averaging the A and B channels at each frequency. After the mean offset and the dipole are removed, the bright (red) emission from the Galaxy dominates the central band of the maps.

BENNETT et al. (see 464, L2)

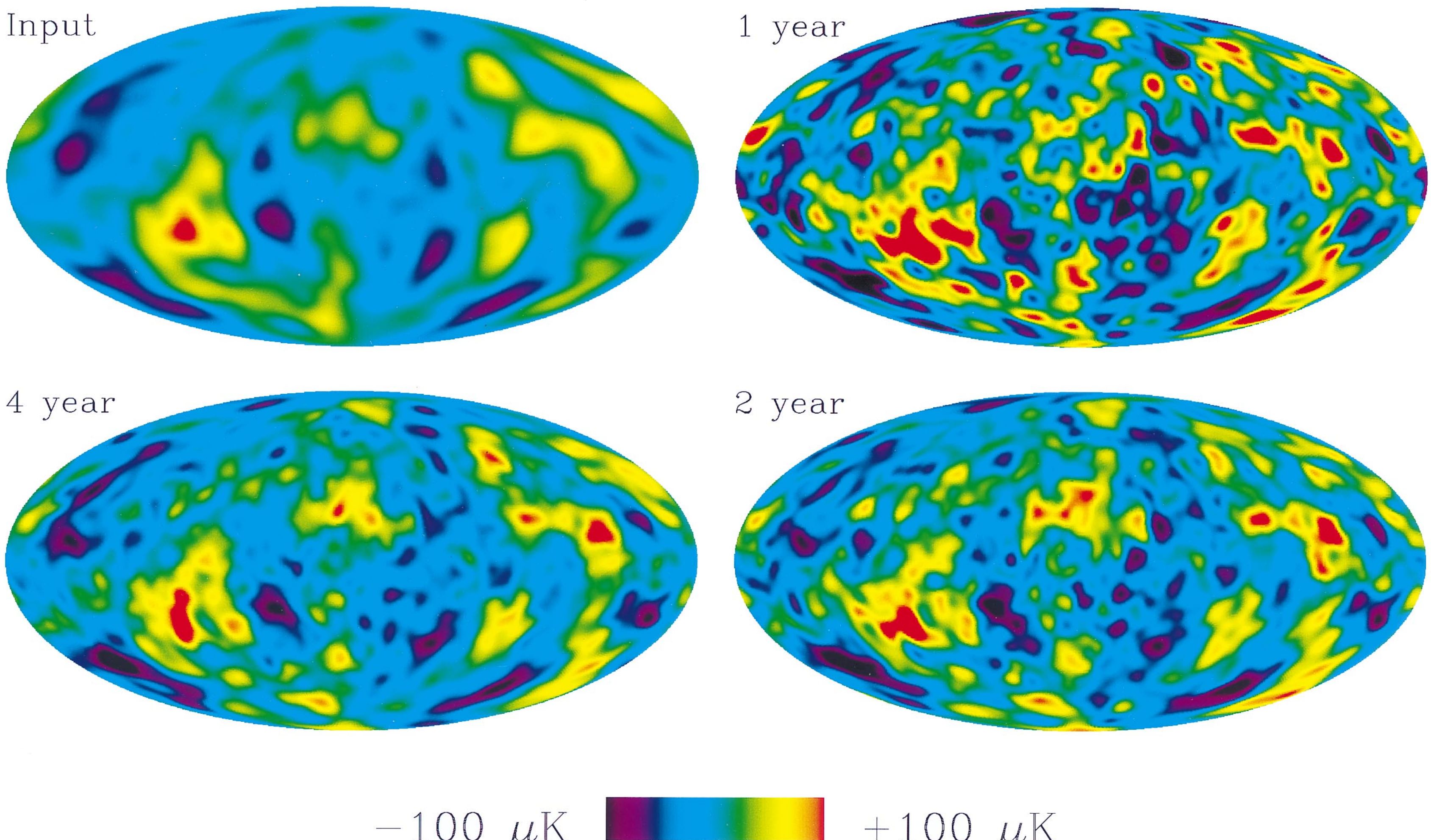

FIG. 2.—(*Top left*) Full-sky simulation of an anisotropy map smoothed to 10° resolution with an $n = 1$ Peebles-Harrison-Zeldovich power spectrum with $Q_{rms-PS} = 18\ \mu K$. DMR instrument noise is added to the sky simulation corresponding to (*top right*) 1 yr; (*bottom right*) 2 yr; (*bottom left*) 4 yr of observations. Note the good visual agreement between the "true" sky on the top left and the 4 yr simulated DMR result on the bottom left.

BENNETT et al. (see 464, L2)

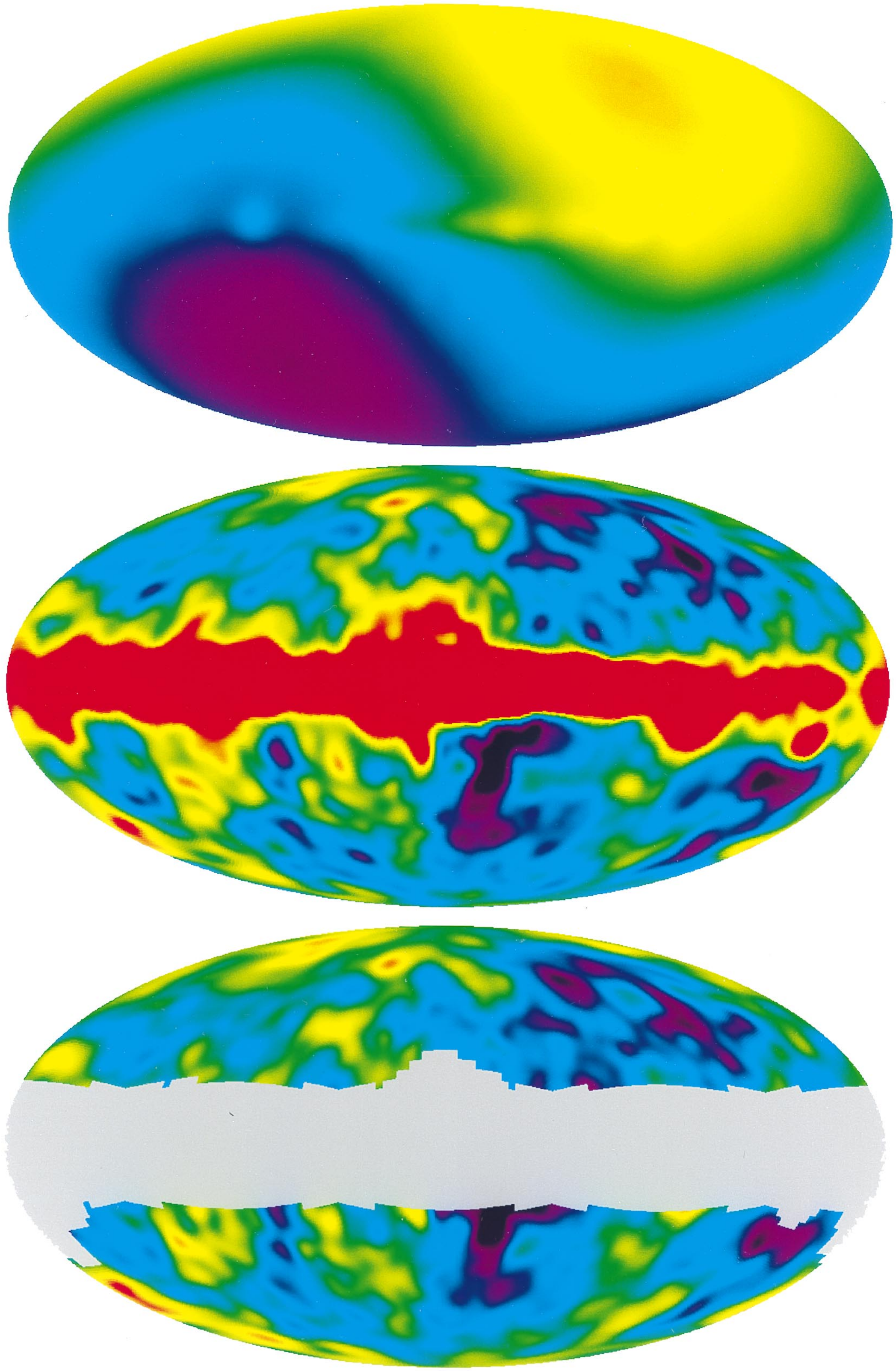

FIG. 4.—(*Top*) Full-sky Mollweide projection of the 4 yr 53 GHz DMR map, including the dipole. (*Middle*) Full-sky Mollweide projection of the 4 yr 53 GHz DMR map, excluding the dipole. (*Bottom*) Full-sky Mollweide projection of the 4 yr DMR map, excluding the dipole, using data from 31, 53, and 90 GHz with modeled Galactic emission removed, and the Galactic custom cut applied.

BENNETT et al. (see 464, L3)